A Multi-Gait Soft Robot

Supporting Information

Robert F. Shepherd[1], Filip Ilievski[1], Wonjae Choi[1], Stephen A. Morin[1], Adam A. Stokes[1], Aaron D. Mazzeo[1], Xin Chen[1], Michael Wang[1] and George M. Whitesides[1,2]*

[1] Department of Chemistry and Chemical Biology, Harvard University,

12 Oxford Street, Cambridge, Massachusetts 02138

[2] Wyss Institute for Biologically Inspired Engineering

60 Oxford Street, Cambridge, Massachusetts 02138

* Corresponding author, email: gwhitesides@gmwgroup.harvard.edu

SI1. Materials and Methods

Soft Robot Fabrication. Masters for the pneu-nets were fabricated in ABS (acrylonitrile butadiene styrene) using a 3D printer (Dimension 3D; Stratasys, Inc.) We molded pneu-nets into a highly extensible, elastomeric material (Ecoflex 00-30 ©; Smooth-On, Inc.) and then layered them onto a relatively inextensible, compliant sheet (PDMS; Sylgard 184, Dow-Corning) (Fig. 1). We then inserted five soft, flexible tubes (1mm I.D., silicone rubber) into a "hub" located at the posterior section of the soft robot; this hub fed the five separate pneu-nets (the tubing was held in place by compression from the surrounding, punctured Ecoflex © silicone rubber). We also fabricated a robot capable of faster crawling locomotion using an extensible elastomer (Ecoflex 00-50 ©; Smooth-On, Inc.) with a larger Young's Modulus than Ecoflex 00-30 ©. The physical dimensions of the robot, as well as the dimensions of the pneu-nets are shown in Fig. S1. Both the Ecoflex elastomers, as well as the Sylgard 184 were cured at 75^{o}C for 60 minutes prior to use. We "glued" the cured Ecoflex layer to the cured Sylgard 184 layer by using a thin, uncured layer of Sylgard 184 as glue; we then allowed the uncured PDMS to permeate into the Ecoflex and Sylgard 184 layers for 60 minutes and finished the bonding of the glue layer by baking the robot in an oven at 75^{o}C for 60 minutes. To increase production throughput, we typically fabricated four robots in parallel.

Manual Control for Obstacle Navigation. We connected the four legs of the robot to Manifold One (M1; manifold here means a group of pressure regulators such as buttons and toggle switches) at pressure, P1, and the spine was connected to either M1 for undulation or Manifold Two (M2) at a lower pressure, P2 (4 psi), for crawling. M1 has

button valves, which allowed the pneu-nets to be pressurized when depressed, and vented to atmospheric when released (Fig. S2). M2 had a switch valve that kept the pneu-nets pressurized until the valve was switched off.

Kinematic Analysis. We determined the speed of actuation of a leg (PN 5) of the tetrapod for different input pressures (Figure S3). We captured video at 200 frames per second (fps) using a high speed video camera (Phantom V7.1; Vision Research) and calculated the time it took for the leg to reach a curvature of 1 cm for pressures varying from 4.5 psi to 20.0 psi. We also tracked the motion of the robot during an undulation and crawling sequence. We used Matlab 2009a's (The Mathworks, Inc.) Image Toolbox to determine the center of mass of the robot (centroid) for each frame of the videos shown in Video S1 and Video S2. We plotted the X- and Y-position of the centroid vs. time for undulation and crawling gaits (Figure S4). For the crawling gait, we inflated the robot's spine after eight seconds and initiated crawling at thirteen seconds. For both gaits, after ~35 seconds, the tether begins to affect the weighting of the centroid and reduces the positional accuracy of our image analysis.

SI2. Calculations of the Bending Stiffness of an Elastomer Membrane with Embedded Pneumatic Channels.

Curvature (κ) of a Pressurized Membrane. Figure S5*A* shows a schematic drawing of an elastomer membrane incorporating embedded pneumatic channels (represented by circles). The bottom layer of the membrane structure is assumed to be unstretchable, but to possess negligible thickness so that the layer does not have significant bending modulus. Pneumatic channels are assumed to be circular for the sake of analytical simplicity. Each of the pneumatic channels is assumed to have infinite length (along the *z*

axis in the figure). In Fig. S5*A*, the pneumatic channels are not pressurized (atmospheric pressure P_{atm} inside the channels) and the membrane is at its resting, flat state (the radius of an undeformed channel is R_{atm}, and length of the membrane = $2R_{atm} \times$ N; N is the number of channels). Fig. S5*B* shows the shape of the membrane when the pneumatic channels are pressurized ($P_1 > P_{atm}$). The channels expand ($R_{atm} \rightarrow R_1$) to adopt the new pressure, leading to a mismatch between the lengths of the membrane along the center of pneumatic channels ($2R_1 \times N$) and along the unstretched bottom layer ($2R_{atm} \times N$). Eq. S1 describes the kinematic correlation between radius of curvature of the membrane ($R_m = 1/\kappa$; see Fig. S5*C* for parameters) and the expansion of the pneumatic cells ($R_{atm} \rightarrow R_1$):

$$\frac{R_m}{R_m - R_1} = \frac{R_1}{R_{atm}} \tag{S1}$$

Eqs. S2 – S5 relate the expansion of pneumatic cells ($R_{atm} \rightarrow R_1$) and the applied pressure (P_1, P_{atm}; Pa or kg m^{-1} s^{-2}), based on the free-body diagram shown in Figure S5*D*: to balance the pressure difference across the walls of pneumatic cells, the tensional force (T; per unit length along z axis; kg s^{-2}) along the wall should be (1):

$$2T = 2R_1(P_1 - P_{atm}) \tag{S2}$$

The constitutive equation Eq. S3 describes the wall-tension T as a function of the strain of the material:(1)

$$T = E \cdot t \cdot \varepsilon \tag{S3}$$

In Equation S3, E (kg m^{-1} s^{-2}), t (m) and ε are the elastic modulus, thickness and strain ($\varepsilon = (R_1 - R_{atm}) / R_{atm}$) of the channel wall, respectively. Stress-strain relationship for elastomers is highly nonlinear – both the elastic modulus of elastomer and the thickness of a channel wall changes as a pneumatic cell is stretched. We ignore these nonlinearities in this analysis as we are interested only in the order of magnitude relationship between the curvature of a membrane and the applied pressure. Combining Eqs. S2 and S3, one can eliminate the term T and obtain a direct relation between the applied pressure and the strain of pneumatic cells:

$$\varepsilon = \frac{R_{atm}(P_1 - P_{atm})}{Et - R_{atm}(P_1 - P_{atm})} \tag{S4}$$

The ratio between radii of the inflated and the original pneumatic cells ($\chi = R_1 / R_{atm} = 1 + \varepsilon$) is then:

$$\chi = \frac{R_1}{R_{atm}} = \frac{Et}{Et - R_{atm}(P_1 - P_{atm})} \tag{S5}$$

Combining Eqs. S1 and S5 leads to an explicit equation that allows us to describe the curvature κ in terms of the expansion ratio χ, and eventually the applied pressure (P_1 - P_{atm}):

$$\kappa = \frac{1}{R_{atm}} \cdot \frac{\chi - 1}{\chi^2} \tag{S6}$$

Fig. S6 shows the curvature of the membrane of typical parameters (E ~ 40 kPa, R_{atm} ~ 1 mm, and t ~ 1 mm) plotted to the difference of pressures ($P_1 - P_{atm}$). The solid line

represents the curvature multiplied by the initial radius of pneumatic cells (R_m) and is non-monotonic. This is because the strain (ε) – and consequently the curvature (κ) of the membrane – increases nonlinearly according to pressure (see Eq. S4). When the pressure is so large that the denominator in Eq. S4 becomes zero, the strain diverges to infinity, and the ratio between the radius of a pneumatic cell and the radius of curvature for the membrane approaches unity ($\kappa \times R_1 \to 1$). In reality, the wall of a pneumatic cell would burst due to the high strain; thus, it should be noted that the approximation based on this analysis is valid only for a low strain regime.

Bending Modulus of the Pressurized Membrane. The other effect of pressurizing pneumatic channels is the increase of the bending modulus (resistance against bending; kg m^{-1} s^{-2}) of the membrane (2). Such stiffening phenomenon is used to make pneumatic structures such as portable pools for kids and camouflage tanks made with balloons (3). This section aims to obtain a qualitative estimate of the bending modulus of a pressurized membrane.

Figure S7 shows three membranes: *A* pressurized only, *B* pressurized and forced to bend further, and *C* pressurized and forced to flatten. The channels of the membranes in Figs. S7*B* and S7*C* become distorted from the original circular shapes into (we assume) ellipses to adopt the change of curvature that is induced by external torque (arrows in the figure). Figure S6*D* illustrates that such change of shapes will increase the area of the walls of pneumatic channels: assuming the air inside the pneumatic channels is incompressible, the volumes inside the circular and elliptic channels is constant (i.e., $\pi R_1^2 = \pi ab$, we assume the channel is infinitely long along the *z* axis in Fig. S7*D*). The

lengths of major and minor axes thus correlate with each other by $b = R_1^2 / a$. The circumference *C* of the ellipse for a given volume is then greater than that of the non-distorted circular pneumatic channel, (i.e., $C > 2\pi R_1$). This rest of section shows that, the more a pneumatic channel is inflated, the more elastic energy is required to cause the same amount of distortion from a circular to elliptic shape. Then it is straightforward that a pressurized membrane is more difficult to bend, because the bending of a membrane leads to the deformation of a channel (circle to ellipse) and thus the change of elastic energy.

Step 1. Deriving the Elastic Energy Associated with the Deformation of a Pneumatic Channel.

Deriving an exact, analytical solution for the circumference of an ellipse is impossible, hence we used the following estimation (4):

$$C \approx \pi\left[3(a+b) - \sqrt{(3a+b)(a+3b)}\right] \tag{S7}$$

When the deformation is infinitesimal (i.e. $a = R_1 \pm \delta$, $\delta << R_1$). $b = R_1^2 / a$ can be approximated to be $b = R_1 \mp \delta$, and Eq. S7 can be re-written as:

$$C \approx \pi\left[6\mathrm{R}_1 - 2\sqrt{4R_1^2 - \delta^2}\right] \approx \pi\left(2R_1 + \frac{1}{2}\delta^2\right) \tag{S8}$$

The circumference in S8 is always greater than that of the original circle ($C > 2\pi R_1$), and consequently, the deformation of a pneumatic channel leads to the corresponding increase of the elastic energy stored by the wall of the pneumatic channel. For the original,

circular shape of a pressurized pneumatic channel, the strain of the wall is given as $\varepsilon = (R_1 - R_{atm}) / R_{atm}$. The elastic potential energy, *PE*, stored in the elastic wall, per channel of unit length along the *z* axis, is then calculated to be:

$$PE = \frac{1}{2} EV\varepsilon^2 \approx E\pi R_1 t\varepsilon^2 \approx E\pi R_1 t\left(\frac{R_1 - R_{atm}}{R_{atm}} \right)^2 \quad \text{(S9)}$$

Here E (kg m^{-1} s^{-2}) is elastic modulus of the elastomer, V (m^3) is the volume of the elastomer, ε is the strain (ratio between the final and the initial lengths). On the other hand, the potential energy *PE'* stored in the elastic wall of the distorted, elliptic channel is (of course, per channel of unit length along the *z* axis):

$$PE' = \frac{1}{2} EV(\varepsilon')^2 \approx E\left(R_1 + \frac{1}{4}\delta^2 \right) t \cdot \left(\frac{\left(R_1 + \frac{1}{4}\delta^2 \right) - R_{atm}}{R_{atm}} \right)^2 \quad \text{(S10)}$$

Dropping higher order terms from Eq. S10, we get Eq. S11:

$$PE' \approx PE + \frac{1}{4} E\delta^2 t\varepsilon^2 \quad \text{(S11)}$$

The volume conservation of the elastomer material requires the wall thickness (t) of an inflated pneumatic channel to be related to the initial thickness at the atmospheric pressure (t_{atm}) as the following:

$$R_1 t = R_{atm} t_{atm} \quad \text{(S12)}$$

Combining Eq. S11 and S12 leads to Eq. S13 that describes the change of elastic energy:

$$PE'-PE = \frac{1}{4}\frac{R_{atm}t_{atm}}{R_1}E\delta^2\varepsilon^2 = \frac{1}{4}\frac{\varepsilon^2}{1+\varepsilon}E\delta^2 t_{atm} \quad \text{(S13)}$$

Eq. S13 shows that, for a pneumatic channel with a given geometry and material property (E, t_{atm}), when the channel is pressurized and strained more (ε becomes higher), the deformation of the pneumatic channel from a circular to an elliptic shape ($R_1 \rightarrow R_1 \pm \delta$) leads to a larger change of elastic energy. That is, the pneumatic channels become stiffer when they are pressurized.

Step 2. Deformation of a Pneumatic Channel due to the Torque-Induced Bending of a Membrane. The next step is to obtain the relation between the bending deformation of the entire membrane and the distortion of a pneumatic channel. One can start from the original relationship between the radius of curvature of a membrane and that of a pneumatic cell (Eq. S1), which is repeated below for convenience:

$$\frac{R_m}{R_m - R_1} = \frac{R_1}{R_{atm}} \quad \text{(S1)}$$

If one forces the membrane to increase or decrease its radius of curvature by a small amount, the lengths of an ellipse (a along the membrane, b perpendicular to membrane) and the radius of curvature of a distorted membrane ($R_m' = R_m \pm \beta$) should hold a similar relation:

$$\frac{R_m'}{R_m'-b} = \frac{a}{R_{atm}} \quad \text{(S14)}$$

Converting Eq. S14 into a differential form, one can obtain:

$$\frac{R_m \pm \beta}{R_m \pm \beta - (R_1 \mp \delta)} = \frac{R_1 \pm \delta}{R_{atm}} \tag{S15}$$

, and combining Eqs. S1 and S15 yields

$$\delta = -\beta \frac{R_1 - R_{atm}}{R_m} \tag{S16}$$

Here the term d represents the deformation of the original, circular channel (radius = R_1) into an elliptical shape (axis lengths = $R_1 \pm \delta$). Combining Eq. S13 and Eq. S16, one can calculate the variation of the potential energy for one pneumatic channel, per given change of radius of membrane curvature β:

$$PE'-PE = \frac{1}{4}\frac{R_{atm}t_{atm}}{R_1} E\delta^2\varepsilon^2 = \frac{1}{4} Et_{atm}\left(\frac{R_{atm}}{R_m}\right)^2 \frac{\varepsilon^4}{1+\varepsilon}\beta^2 \tag{S17}$$

meaning the change of elastic energy (*PE' – PE*) due to the torque-induced bending of the membrane ($R_m \rightarrow R_m \pm \beta$) is highly dependent on the pre-strain (ε) of the pneumatic channels that was caused by the pressure. In short, pressurized membranes become stiffer.

SI5. References

1. Timoshenko SP (1970) Theory of Elasticity (McGraw-Hill).
2. Tabata O, Konishi S, Cusin P, Ito Y, Kawai F, Hirai S, Kawamura S (2001) Micro fabricated tunable bending stiffness devices. *Sensors and Actuators A* 89 119-123
3. Chi JY and Paulettie RMO (2005) An outline of the evolution of pneumatic structures. *II Simposio Latinoamericano de Tensoestructuras Caracas*, Venezuela, May 4-5 2005, http://www.lmc.ep.usp.br/people/pauletti/Publicacoes_arquivos/Chi-and-Pauletti.Pdf

4. Almkvist G, Berndt B Gauss (1988) Landen, Ramanujan, the Arithmetic-Geometric Mean, Ellipses, Pi, and The Ladies Diary. *American Mathematical Monthly*, 95:585-608

Figure Legends

Fig. S1. ***A*** Top view of the quadruped, with dimensions in millimeters. The length of the robot is 135.7 mm, the width 58.5 mm. ***B*** The side view of PN 3, showing the thickness of the Ecoflex layer (Layer 1) to be 5.3 mm, the pneu-net channel thickness to be 0.5 mm, the channel connecting the pneu-nets to be 1.0 mm thick, and the Sylgard 184 (Layer 2) strain limiting layer to be 1.0mm.

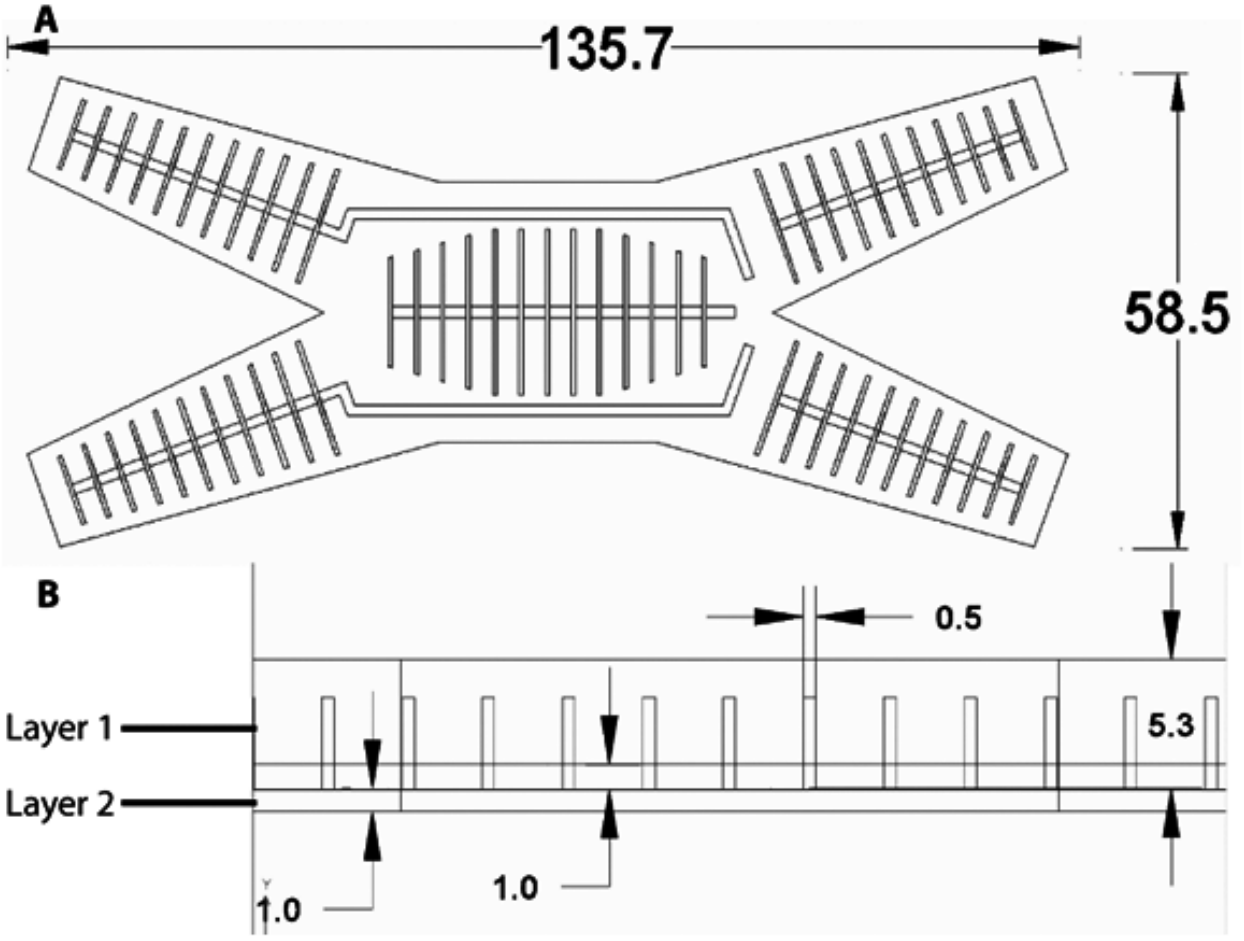
A
135.7
58.5
B
0.5
Layer 1
Layer 2
5.3
1.0
1.0

Fig. S2. ***A*** *Computer control*. Schematic diagram of a system of solenoid-valves controlled via computer. The computer is programmed to actuate the soft robot in undulation or crawling gait at a pressure of 7 psi. ***B*** *Manual control*. Schematic diagram of a system of spring-valves controlled via manual operation (depressing the spring-valve actuates the corresponding pneu-net). The valve configuration for (top) undulation gait requires a valve for each pneu-net and uses a pressure of 7 psi. The (bottom) crawl gait uses an individual valve for PN -1, -2, -4, and -5. PN 3 is held at a constant pressure of 4 psi. The direction of the pressurized air-flow is indicated by the arrow direction and the solenoid-valves are represented by a slanted line in a circle and the spring-valves are represented by a zig-zagged line in a circle.

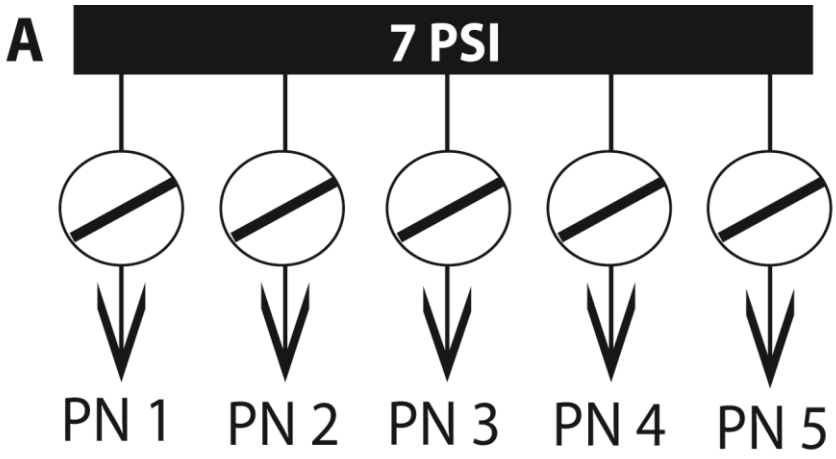
A
7 PSI
PN 1
PN 2
PN 3
PN 4
PN 5

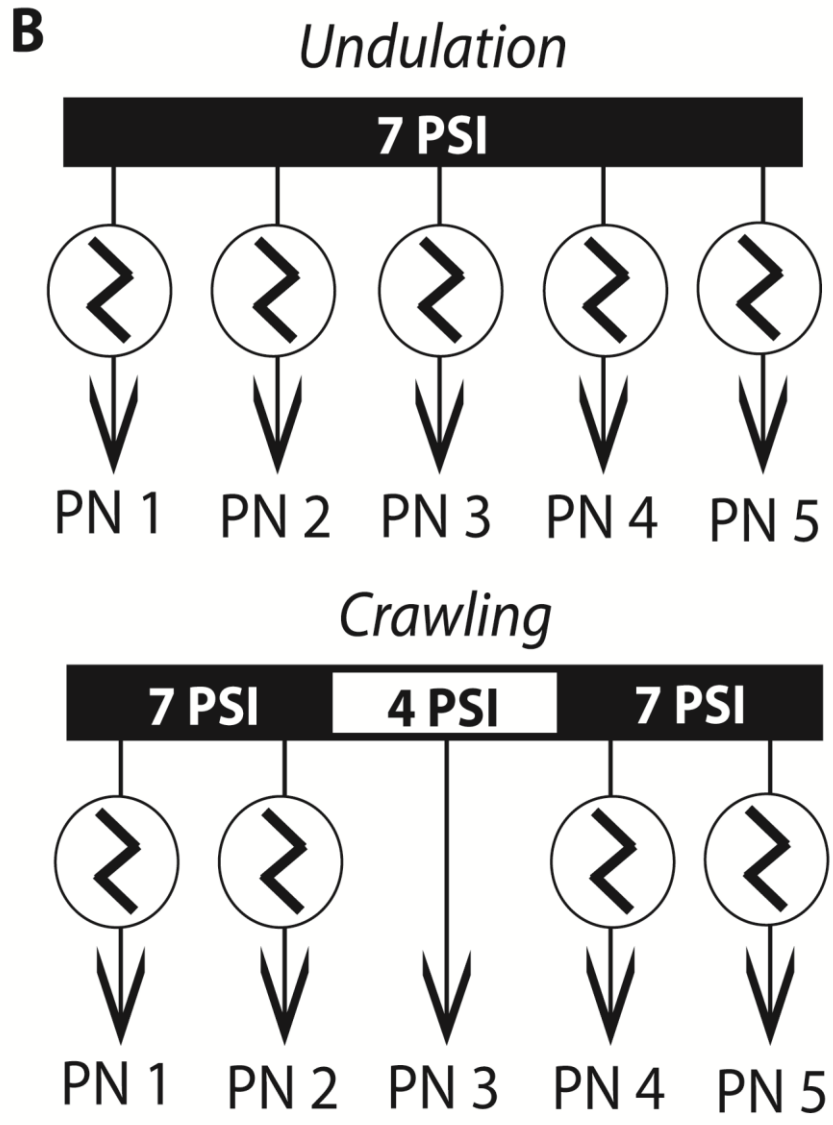
B
Undulation
7 PSI
PN 1
PN 2
PN 3
PN 4
PN 5
Crawling
7 PSI
4 PSI
7 PSI
PN 1
PN 2
PN 3
PN 4
PN 5

Fig. S3. Time to actuate (squares) and de-actuate (circles) PN 5 to a 1cm radius of curvature. Error bars are for n = 7 replicates. Data obtained using high speed video (Phantom V7.1) at 200 fps.

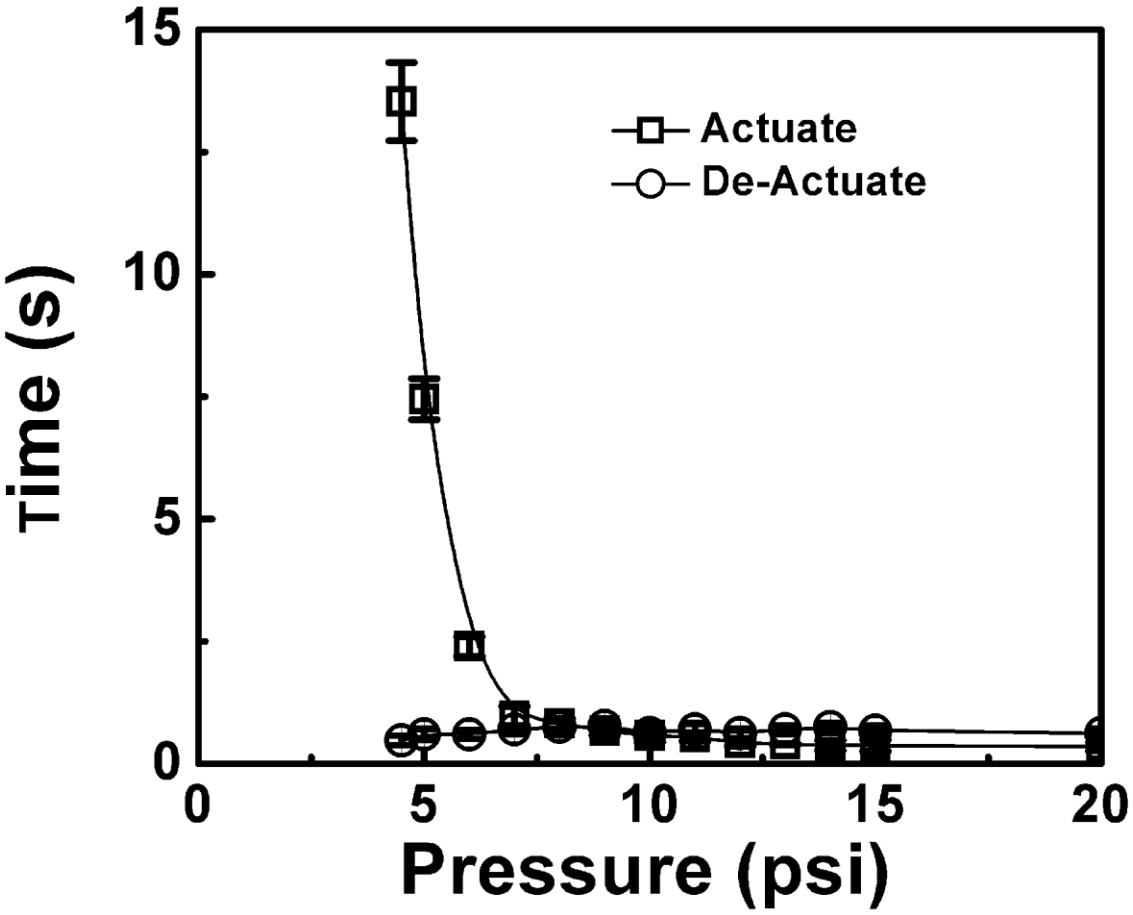
15
10
5
0
Time (s)
0
5
10
15
20
Pressure (psi)
Actuate
De-Actuate

Fig. S4. The x and y position of the center of mass of the robot vs. actuation time for ***A*** undulating and ***B*** crawling gait. Obtained using Matlab R2009a image analysis on Video S1 and Video S2.

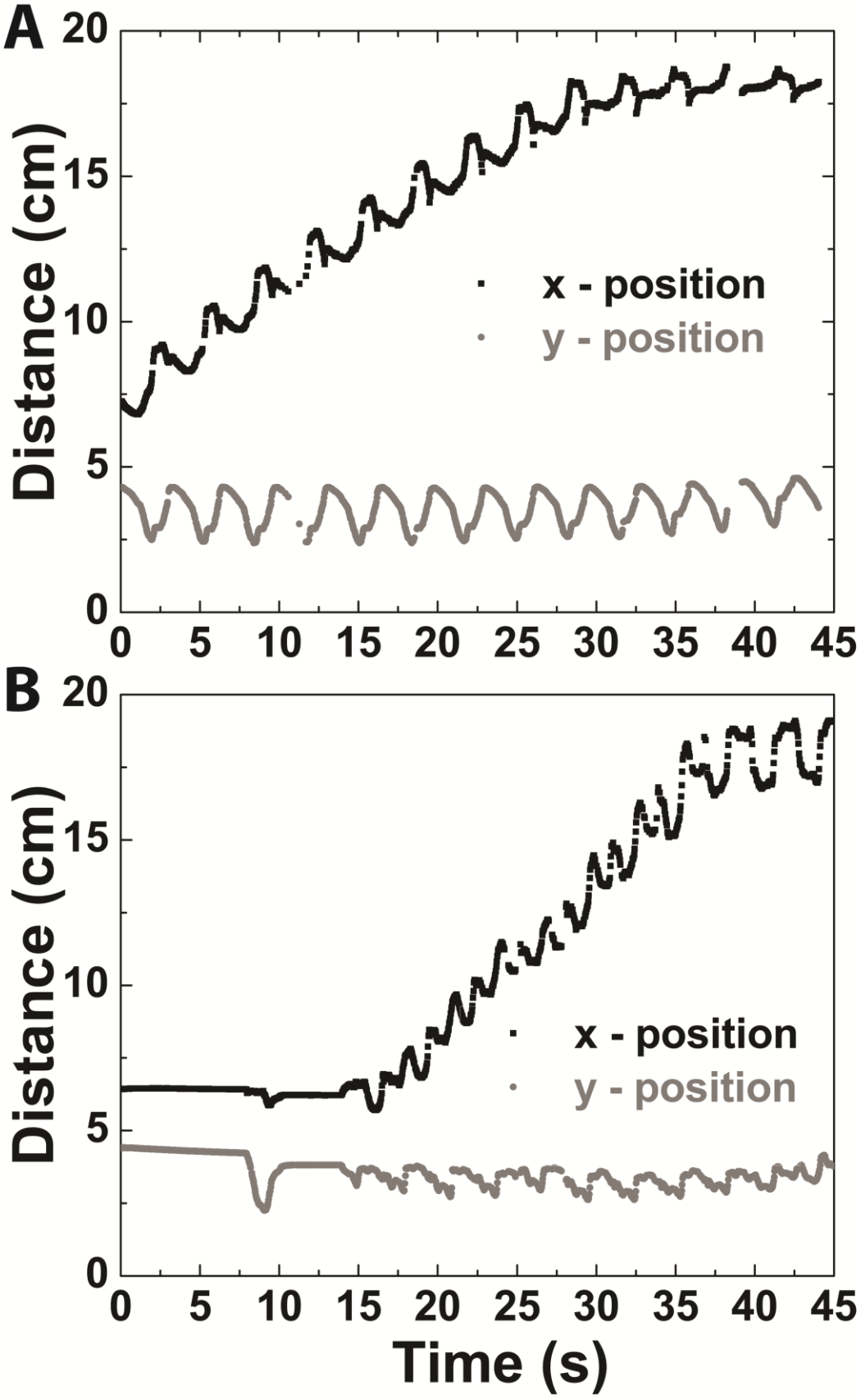
A
B
Distance (cm)
Time (s)
x - position
y - position
0
5
10
15
20
25
30
35
40
45

Figure S5. ***A*** schematic illustrating an elastomer membrane with N pneumatic channels. Circles represent pneumatic channels, possessing infinite length along the *z* axis. The pressure inside the pneumatic channels is atmospheric, and the membrane is at its resting state. ***B*** Same membrane at its pressurized state ($P_1 > P_{atm}$). Pneumatic channels now have larger radius R_1 and the membrane spontaneously bends upward due to the mismatch between the lengths of the bottom layer ($2R_{atm} \times N$) and along the pneumatic channels ($2R_1 \times N$). ***C*** A free-body diagram of an upper half of a pressurized pneumatic channel. ***D*** Parameters of a pressurized membrane.

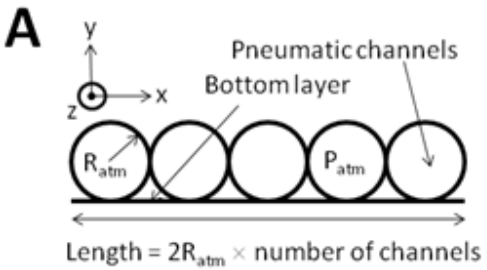
A
y
x
z
Pneumatic channels
Bottom layer
R_{atm}
P_{atm}
Length = $2R_{atm}$ × number of channels

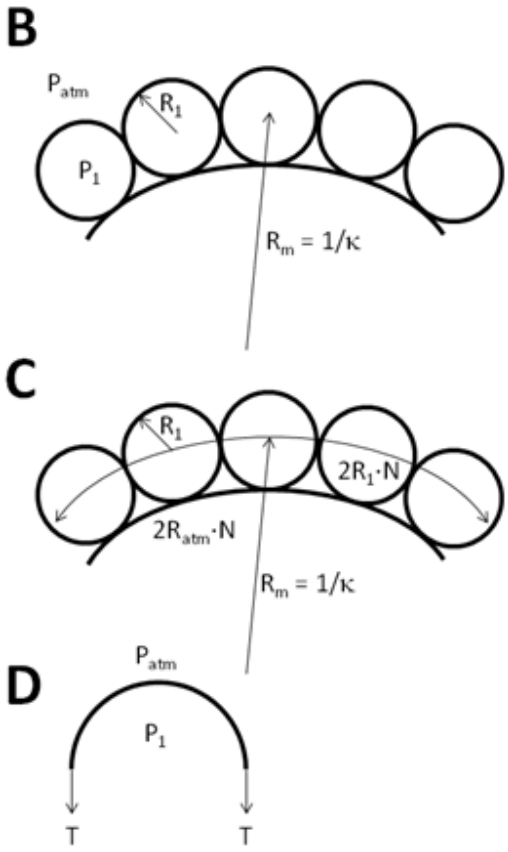
B
P_{atm}
R_1
P_1
$R_m = 1/\kappa$
C
R_1
$2R_1 \cdot N$
$2R_{atm} \cdot N$
$R_m = 1/\kappa$
D
P_{atm}
P_1
T
T

Figure S6. Curvature of a membrane plotted with respect to the pressure difference ($P_1 - P_{atm}$); the parameters for the membrane were E = 40 kPa, R_{atm} = 1 mm, and t = 1 mm. Circles represent pneumatic channels, possessing infinite length along the z axis. The solid line represents the curvature multiplied by the initial radius of the pneumatic cells and the dashed line represents the curvature multiplied by the final radius of the pneumatic cells.

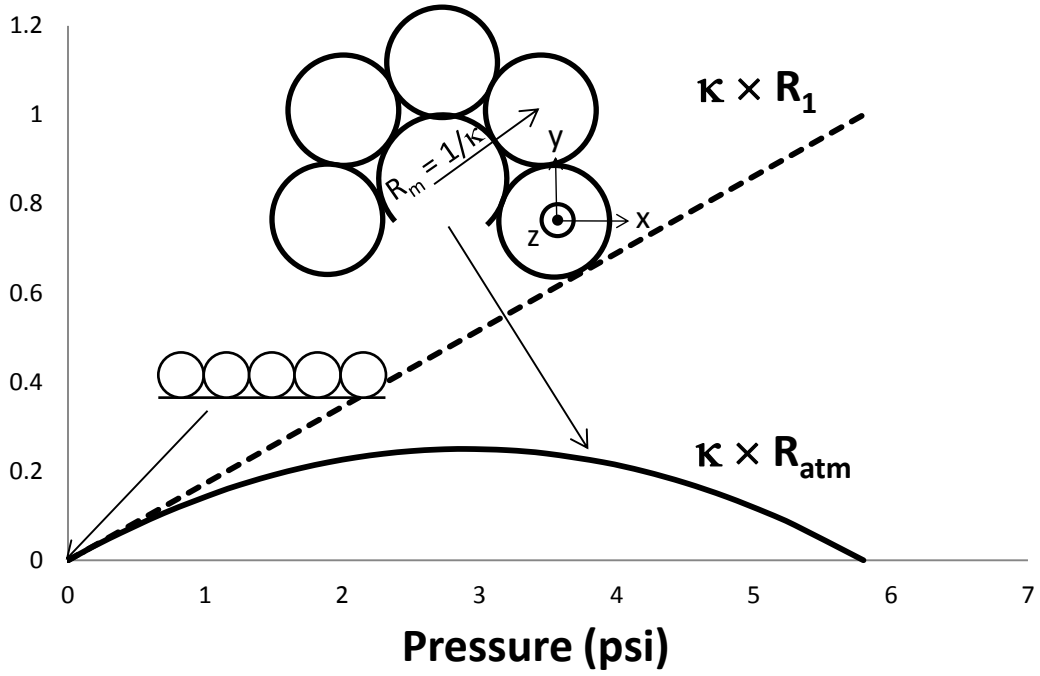
1.2
1
0.8
0.6
0.4
0.2
0
0
1
2
3
4
5
6
7
κ × R1
κ × Ratm
Rm = 1/κ
y
x
z
Pressure (psi)

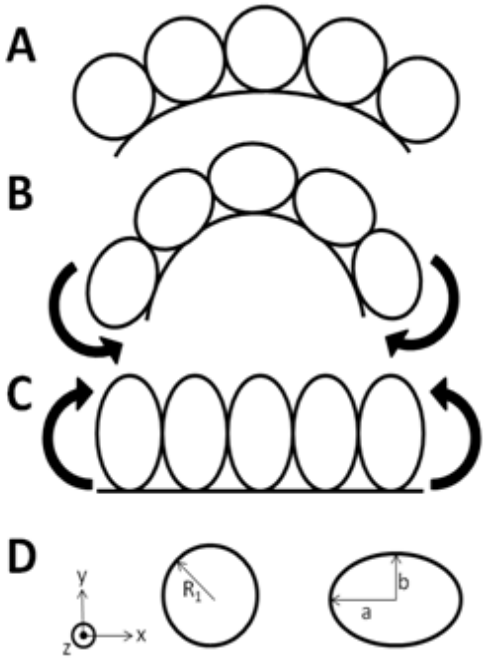

Figure S7. Schematics showing pressurized membranes, ***A*** without additional torque, ***B*** with a torque that further bends or ***C*** flattens the membranes. Black arrows indicate the direction of the applied torque. ***D*** Cross-sectional shapes of undistorted (left) and distorted (right) pneumatic channels.

Video S1. Real time video of soft robot undulation.

Video S2. Real time video of soft robot crawling.

Video S3. Real time video of soft robot crawling using high modulus (Ecoflex 00-50 ©) pneu-nets.

Video S4. Real time video of the soft robot transitioning from crawling to undulating and back to crawling in order to navigate an obstacle: a glass plate elevated 2 cm from the ground.